Tunable Anisotropic Wettability of Rice Leaf-Like Wavy Surfaces

*Seung Goo Lee, Ho Sun Lim, Dong Yun Lee, Donghoon Kwak, and Kilwon Cho**

Rice leaves can directionally shed water droplets along the longitudinal direction of the leaf. Inspired by the hierarchical structures of rice leaf surfaces, synthetic rice leaf-like wavy surfaces are fabricated that display a tunable anisotropic wettability by using electrostatic layer-by-layer assembly on anisotropic microwrinkled substrates. The nanoscale roughness of the rice leaf-like surfaces is controlled to yield tunable anisotropic wettability and hydrophobic properties that transitioned between the anisotropic/pinned, anisotropic/rollable, and isotropic/rollable water droplet behavior states. These remarkable changes result from discontinuities in the three-phase (solid–liquid–gas) contact line due to the presence of air trapped beneath the liquid, which is controlled by the surface roughness of the hierarchical nanostructures. The mechanism underlying the directional water-rolling properties of the rice leaf-like surfaces provides insight into the development of a range of innovative applications that require control over directional flow.

1. Introduction

Anisotropic wettability on patterned surfaces has attracted considerable attention because of its potential applications to microfluidic devices and directional flow control devices, in which liquids are driven along a preferred direction.[1–12] Anisotropic wettability can be achieved through chemically[1–3] or geometrically[4–10] anisotropic heterogeneous surfaces. Liquids on the surfaces of anisotropic patterns tend to move more easily along a direction parallel, rather than perpendicular, to the patterns due to the lower energy barrier for wetting;[3,6,7] however, although the anisotropic wettability of geometrical structures has been widely studied using single-level anisotropic structures, the anisotropic wettability of dual- or multi-level structures has not been examined extensively.

Natural multiscale structured surfaces are central to understanding unusual superhydrophobic behavior.[13–16] For example, rice leaves directionally shed water droplets along the longitudinal direction of the leaf. Anisotropic droplet rolling (i.e., dewetting) has been explained in terms of the quasi-one-dimensional arrangement of micropapillae covered with nanoscale wax features along the longitudinal direction of the leaf to enable water droplets to easily roll off along a single direction.[16] Several artificial surfaces inspired by the hierarchical structures of rice leaf surfaces have been developed using various methods, including micromolding,[17] nanoimprint lithography,[18] and photolithography.[19,20] Most previous rice leaf-inspired surface preparations have attempted to achieve static wetting anisotropy or the distortion of water droplets. Dynamic anisotropic water droplet behavior has not yet been studied because the high contact angle hysteresis achieved in previous studies tended to hold water droplet in a pinned state. Specially-designed surfaces with rice leaf-inspired multiscale structures that yield superhydrophobic properties have been fabricated,[8,20] and the effects of the microgroove array heights and widths (or aspect ratios) on the anisotropic rolling properties have been described; however, no studies have yet demonstrated how control over the submicroscale or nanoscale features of a fixed anisotropic wavy microstructure affect the anisotropic wettability or dynamic behavior of water droplets.

This paper explores the properties of hierarchical one-dimensional wavy structured rice leaf surface topographies. Inspired by the unique structure, we prepared artificial rice leaf surfaces with surface structures in which the number of nanoporous multilayers on a given wavy microstructure was controlled. The fabrication method involved a combination of surface wrinkling and electrostatic layer-by-layer (LBL) assembly. The microscale roughness was held constant using the properties of the anisotropic wrinkling patterns.[21–24] The LBL assembly was then used to fabricate nanoporous multilayers on the anisotropic wrinkling patterns to provide controlled surface roughness and porosity via the pH and number of polyelectrolyte and nanoparticle deposition cycles.[25–30] The fabricated surfaces exhibited a range of wettability states (anisotropic/pinned, anisotropic/rollable, or isotropic/rollable state), depending on the surface roughness of the hierarchical nanostructures. These findings support the observation that multiple roughness levels in the anisotropic rice leaf microstructures played an essential role in the water repellence and anisotropic droplet rolling behavior.

2. Results and Discussion

Rice leaf blades (*Oryza sativa*) are long, narrow, and superhydrophobic, displaying water contact angle (CA) greater than

Dr. S. G. Lee, Dr. H. S. Lim, Dr. D. Y. Lee,
Dr. D. Kwak, Prof. K. Cho
Department of Chemical Engineering
Pohang University of Science and Technology
Pohang, 790-784, Korea
E-mail: kwcho@postech.ac.kr

DOI: 10.1002/adfm.201201541

© 2013 WILEY-VCH Verlag GmbH & Co. KGaA, Weinheim

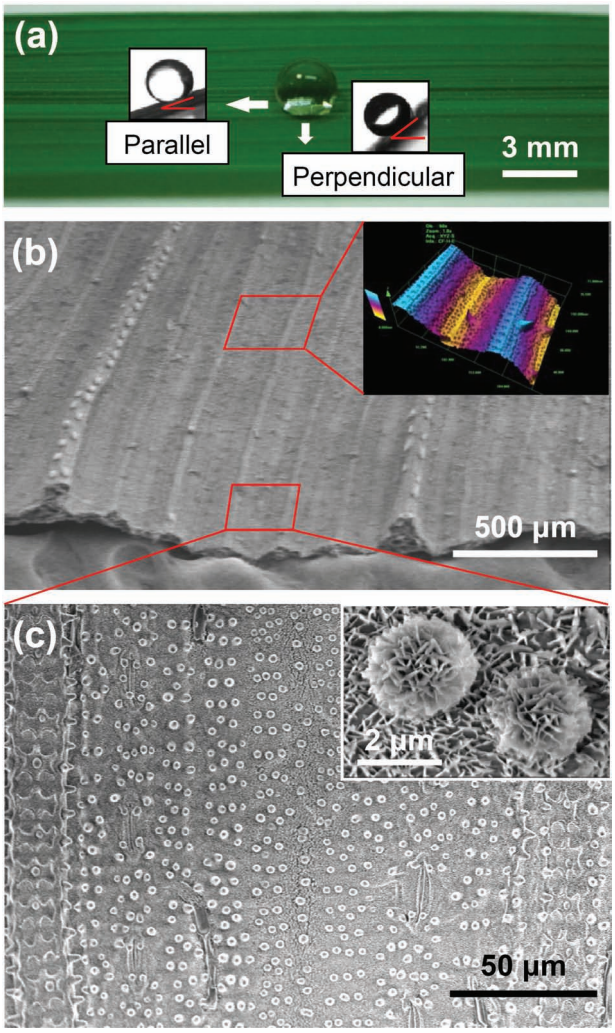

Figure 1. Rice leaf surfaces exhibit anisotropic rolling behavior. a) A droplet of water on a rice leaf. The insets show optical images of a roll-off angle measurement for a water droplet (volume of 4 µL) parallel or perpendicular to the rice leaf longitudinal direction. b) A tilted SEM image of the upper surface of the rice leaf. The inset shows a CLSM topographical image of the rice leaf surface. c) A magnified image of (b). The inset shows a magnified image of the papillae covered by wax.

150° and anisotropic wetting (**Figure 1**a and Figure S1b in the Supporting Information). Interestingly, the roll-off angle (i.e., the critical angle at which a water droplet begins to roll on a tilted surface) parallel to the longitudinal direction of the leaf was much smaller than the roll-off angle perpendicular to this direction (see the insets of Figure 1a). As with the properties of lotus leaves (Figure S2b in the Supporting Information), this anisotropic rolling property facilitates effective self-cleaning and draining processes.

The anisotropic rolling behavior of water droplets originated from the physical multiscale roughness and the chemical hydrophobicity. The upper (adaxial) surface of a rice leaf was characterized by scanning electron microscopy (SEM) and confocal laser scanning microscopy (CLSM). The leaf surface displayed many parallel ridges formed by vascular bundles (VB) and wavy mesophyll layers with an average ridge period of 185 µm and a height of 46 µm (small VB) or 132 µm (large VB) (see Figure 1b). Further magnified views displayed a number of papillae 2 µm in diameter and 4 ± 1 µm in height, arranged in a direction parallel to the ridge direction (Figure 1c). The nanoscale waxes were densely dispersed over the surface, resulting in a hierarchically structured superhydrophobic surface similar to the lotus leaf (inset, Figure 1c and Figure S2a in the Supporting Information). These observations indicated that the anisotropic rolling properties resulted from the unique surface topography, comprising hierarchical structures on anisotropic wavy microstructures.

The ability of the hierarchical anisotropic wavy microstructures to support directional water shedding was investigated by designing and preparing artificial rice leaf-like surfaces. The process by which the rice leaf-like surfaces were fabricated is schematically illustrated in **Figure 2**a. The microwrinkles were fabricated by exposing uniaxially stretched poly(dimethylsiloxane) (PDMS) to ultraviolet-ozone (UVO) radiation, after which the strain was released. The wrinkled patterns were generated perpendicular to the pre-strain direction as a result of the mismatched elastic moduli of the relatively stiff silicate-like top layer and the soft compliant PDMS substrate (see the Supporting Information for more details).[22–24] The cross-sectional SEM images in Figure 2b show that the surface consisted of periodically wavy microstructures with a period of 41 µm and a height of 7 µm. These wrinkled substrates were homogeneous and crack-free due to the mild preparation conditions.

The surface roughness of the samples was enhanced by applying LBL assembly, in which wrinkled substrates with a negatively charged surface were alternately immersed in aqueous solutions of poly(allylamine hydrochloride) (PAH, $\overline{M}_w$ = 70 000 g/mol) or SiO_2 nanoparticles (SN, 11 nm in diameter, see the Experimental Section for additional details).[29,30] Upon completion of the SiO_2 nanoparticle deposition processes, the surfaces were made hydrophobic by vapor deposition of (tridecafluoro-1,1,2,2-tetrahydrooctyl)dimethylchlorosilane. The features of the nanostructures with $(PAH/SN)_5$ on the microwrinkled surfaces are shown in the CLSM image of Figure 2b. The surface morphology included hierarchical structures that resembled the surface morphologies of rice leaves. The aggregated nanoparticles imparted a multiscale roughness and high porosity consisting of submicroscale nanopores. As shown in Figure 2c–e, as the number of PAH/SN bilayers increased to 2, 5, and 9, the surface roughness increased, and nanopores were formed accordingly. CLSM was used to quantitatively determine the surface roughness of the hierarchical nanostructures. As the number of PAH/SN bilayers on the wrinkled PDMS substrate was increased from 0 to 12, the root-mean-square (RMS) roughness (R_q) systematically varied from 21 to 138 nm (Figure S4 in the Supporting Information). These results suggested that the surface roughness and nanoporosity of the UVO-treated PDMS surface could be controlled within tens of nanometers.

The anisotropic wetting of the fabricated surfaces was investigated by measuring the static water CAs both perpendicular ($\theta_\perp$) and parallel ($\theta_{//}$) to the direction defined by the grooves. As shown in **Figure 3**a, the static CAs increased and reached

© 2013 WILEY-VCH Verlag GmbH & Co. KGaA, Weinheim

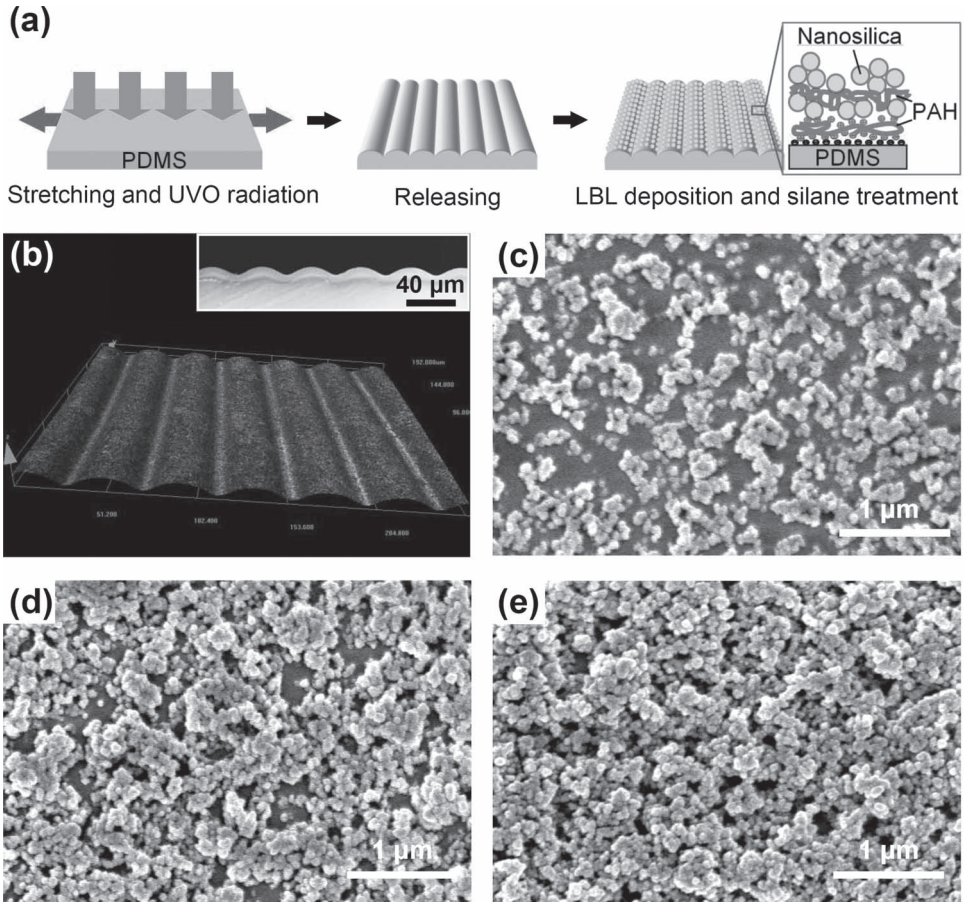

Figure 2. Fabrication of the rice leaf-like surfaces. a) Schematic illustration of the fabrication process comprising surface wrinkling, LBL deposition, and treatment of the PDMS film. b) CLSM image of the fabricated rice leaf-like surfaces. The inset shows a cross-sectional SEM image of a wavy PDMS substrate. c–e) SEM images of the nanostructured films on PDMS substrates with a different number of deposition cycles; (c), (d), and (e) indicate 2, 5, and 9, respectively.

a saturating value as the surface nanostructure roughened (i.e., the $(PAH/SN)_n$ increased). Initially, a film of $(PAH/SN)_0$ on the wavy PDMS had a $\theta_\perp$ of 130° ± 2° and $\theta_{//}$ of 112° ± 1° at small RMS roughness values (R_q of 20 nm) of the surface. This strong anisotropic wetting properties resulted from the directional pinning barrier caused by the wrinkle heights, in agreement with the findings of Chung et al.[7] Both $\theta_\perp$ and $\theta_{//}$ increased with increasing R_q, then saturated at an R_q of 100 nm ($\theta_\perp = \theta_{//} = 175° \pm 1°$). Furthermore, as R_q increased, the difference between $\theta_\perp$ and $\theta_{//}$ gradually decreased, finally reaching 0°, i.e., the wettability transitioned from anisotropic to isotropic, even if the wrinkles retained their anisotropic microstructures. These results indicated that the anisotropic wettability could be overwhelmed by the superhydrophobicity of the surfaces.

To investigate the anisotropy of the dynamic water droplet behavior, we measured the perpendicular and parallel roll-off angles of 4 μL water droplets on the fabricated surfaces. The trend in the roll-off angle resembled that of the CA hysteresis (i.e., the difference between the advancing and receding CAs), and both roll-off angles and CA hysteresis displayed three distinct regimes (see Figure 3b,c). The roll-off angle is closely related to the volume (or mass) of the water droplet and the water repellency of the surface. This relationship is given by[31]

$$\sin\alpha = \frac{w\gamma_{LV}}{mg}(\cos\theta_r - \cos\theta_a), \quad (1)$$

where α is the roll-off angle, w is the width of the droplet, γ_{LV} is the interfacial tension between the liquid and vapor, mg is the gravitational force due to the mass of the droplet, and θ_a and θ_r are the advancing and receding CAs, respectively. In this equation, the roll-off angle is related with the balanced force along the roll-off direction, including the gravitational force of the droplet and the restraining force caused by CA hysteresis. Therefore, the CA hysteresis determines the mode of action in water droplets of a given volume. At low surface roughness values (regime I), a large CA hysteresis pins water droplets on the surface, whereas the small anisotropic CA hysteresis generates directional movement of the water droplets, as observed on rice leaves (regime II). The sample with an R_q of 40 nm displayed roll-off angles along the parallel and perpendicular directions that differed by 18°, comparable to the difference observed on natural rice leaves (16°). Thus, our fabricated

© 2013 WILEY-VCH Verlag GmbH & Co. KGaA, Weinheim

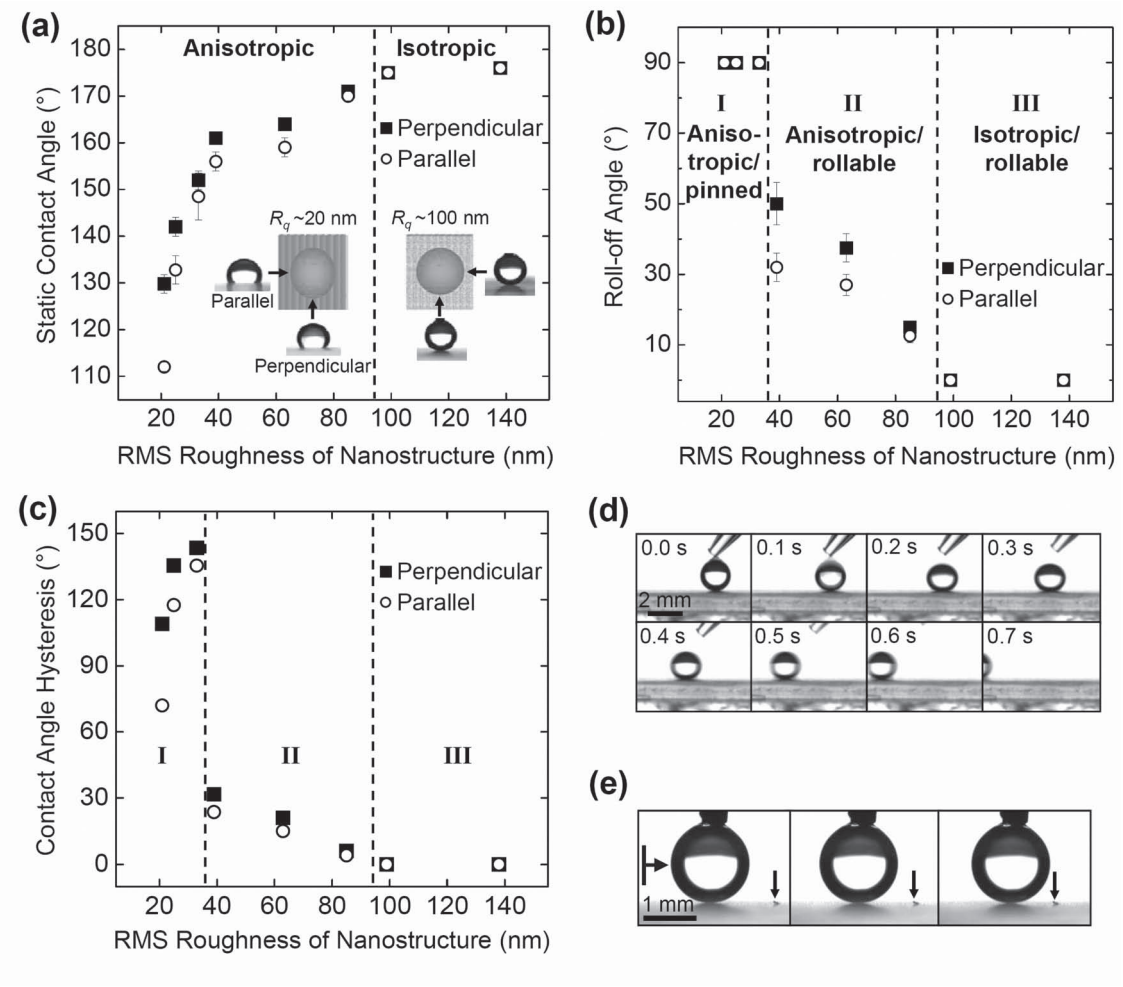

Figure 3. a–c) Static water contact angles (a), roll-off angles (b), and contact angle hysteresis (c) perpendicular (black squares) or parallel (white dots) to the longitudinal direction of the rice leaf-like surfaces as a function of the RMS roughness (R_q) of the surface nanostructures. The insets of (a) show water droplets on surfaces tilted along the parallel or perpendicular directions on differently structured surfaces with R_q of 20 nm (left) or R_q of 100 nm (right). A roll-off angle of 90° in (b) indicates that the droplet did not fall, even if the substrate were tilted until vertical. d) A series of photographs of a rolling water droplet on a surface with an R_q of 100 nm. e) A series of photographs showing the drag movement of a water droplet on a fabricated surface with an R_q of 100 nm.

surfaces successfully mimicked the directional water-rolling properties of rice leaves. Water droplets on the very rough surfaces (regime III) rolled off without any specific directionality at an extremely small roll-off angle, below 1°, as a result of the extremely small values of CA hysteresis, as predicted in Equation 1 (see Figure 3d). In this regime, the water droplets moved along the directions both perpendicular and parallel to the grooves while maintaining a perfect solid ball shape without any apparent deformation (see Figure 3e). The roll-off angles and CA hysteresis properties shown in Figure 3b,c, indicated that the dynamic water droplet behavior may be systematically tuned between anisotropic/pinned, anisotropic/rollable, and isotropic/rollable states simply by varying the surface roughness of the hierarchical nanostructures on a fixed anisotropic wavy microstructure.

As described above, the roll-off angle is closely related to the volume of a water droplet and the water repellency of a surface. **Figure 4** shows the perpendicular and parallel roll-off angles as a function of the water volume for surfaces fabricated in the water-rollable regime, with R_q above 35 nm. The various surfaces in regime II (with R_q of 40, 63, or 85 nm) exhibited both anisotropic and isotropic rolling behavior with distinct or convergent roll-off angles along the parallel and perpendicular directions (see Figure 4a–c). On the other hand, any water droplet (on the μL scale in this study) on a rough surface in regime III (R_q > 95 nm) rolled off freely without rolling anisotropy. Interestingly, the critical water volume at which the parallel and perpendicular roll-off angles converged decreased as the surface roughness increased. The critical water volume decreased from 35 μL (R_q of 40 nm) to less than 1 μL (R_q > 95 nm). According to Equation 1, as the droplet volume increases or the CA hysteresis decreases, the effects of the mass become more dominant than the surface tension effects, which leads to an easy transition from anisotropic to

© 2013 WILEY-VCH Verlag GmbH & Co. KGaA, Weinheim

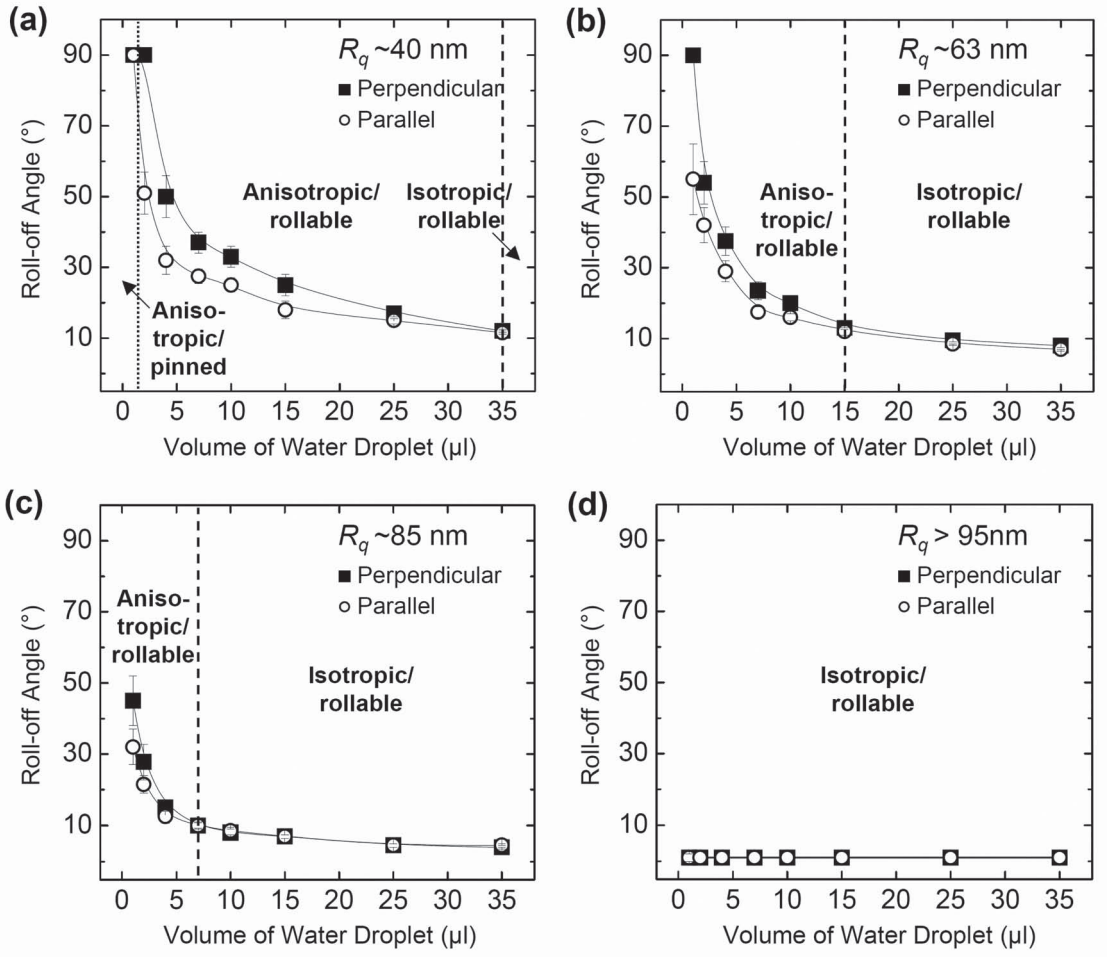

Figure 4. Roll-off angles along the directions parallel or perpendicular to the anisotropic structures as a function of the water volume for rice leaf-like surfaces in the water-rollable regime. The RMS roughness values of the surface nanostructures for (a), (b), (c), and (d) were 40, 63, 85, and above 95 nm, respectively. A roll-off angle of 90° indicates that the droplet did not fall, even if the substrate were tilted until vertical. The parallel and perpendicular roll-off angles converged at a critical water volume (dashed lines).

isotropic rolling behavior. This result agreed with the transition of water-rolling behavior observed previously for anisotropic structures[6,20] and real rice leaves (see Figure S1c in the Supporting Information). These results suggested that the anisotropic rolling behavior could be changed to isotropic rolling behavior for water on rice leaf-inspired surfaces, provided that the droplets maintained sufficiently large in the water-rollable state.

The three types of water droplet behavior (anisotropic/pinned; anisotropic/rollable; isotropic/rollable, I–III in Figure 3) with different water contact angles could be explained in terms of the distinct contact modes and the discontinuous three-phase (solid–liquid–gas) contact line (TCL).[32–43] Possible solid–water contact modes from the top and side views, and the in situ OM images of the interface between the fabricated surface and the water droplet are shown in **Figure 5**. Unlike pillar-like anisotropic structures with vertical walls,[6] water droplets on the wrinkled PDMS surfaces were in the fully wetted Wenzel state[32] because the transition between the Wenzel state (lower energy state) and the air-trapped Cassie state (higher energy state)[33] was barrierless and the Laplace pressure required for maintaining the Cassie state was reduced by the largely inclined side walls of the wrinkled PDMS (see the Supporting Information for more details).[42] A droplet in the Wenzel state was strongly pinned to the surface with a high water adhesion due to the continuous and stable TCL (Figure 5(I)), whereas a droplet in the Cassie state easily rolled off the surface with R_q > 35 nm due to a discontinuous TCL and the large volume of air trapped beneath the liquid (see the arrow in Figure 5(II)). In addition, the CA hysteresis and roll-off angle perpendicular to the grooves were higher than the values parallel to the grooves because the TCL for water droplet movement perpendicular to the grooves was more discontinuous than that parallel to the grooves due to the higher wetting/dewetting energy barrier (Figure 5(II)).[6] As the surface roughness of the nanostructures (i.e., hydrophobicity or the area fraction of the water–air interface) increased, the initial anisotropy of the TCL decreased, promoting a transition in the water rolling behavior from anisotropic to isotropic due to the

© 2013 WILEY-VCH Verlag GmbH & Co. KGaA, Weinheim

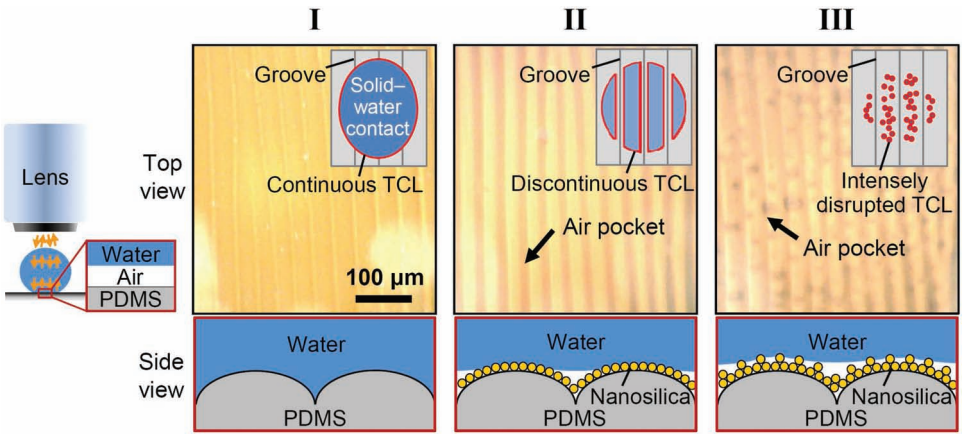

Figure 5. The OM images of the three-phase interface beneath a water droplet for various values of R_q: (I) 20 nm, (II) 40 nm, (III) 100 nm. Schematic illustrations of the possible solid–water contact modes on three surfaces (I–III) in Figure 3 (top and side views).

point solid–water contact mode resulting from the disrupted TCL (Figure 5(III)).[43] These remarkable changes resulted from discontinuities in the TCL due to the fraction of trapped air beneath the liquid, which was controlled by surface roughness of the hierarchical nanostructures.

According to our results, a variety of water droplet behavior on leaf surfaces may be explained in terms of competition between the anisotropic wettability and the water repellency. As the surface roughness of the nanostructures (e.g., waxes) increased or the anisotropy of the structures decreased, the water droplets on the surfaces showed weak anisotropic rolling, thereby displaying isotropic/rollable behavior similar to that observed on lotus leaves. By contrast, if the surface roughness of a nanostructure was too small and the structures were highly anisotropic, the surface exhibited anisotropic/pinned behavior (Figure S6 in the Supporting Information). A sufficiently high (but not too high) nanostructure surface roughness on an anisotropic microstructure was shown to play an important role in inducing anisotropic water-rolling behavior for the effective self-cleaning of rice leaves.

3. Conclusions

Inspired by the surfaces of rice leaves, which feature hierarchical nanostructures on anisotropic wavy microstructures, we prepared rice leaf-like surfaces with tunable anisotropic wettability properties through a combination of LBL assembly and surface wrinkling. We systematically tested and quantified the effects of the hierarchical nanostructure surface roughness on the anisotropic wettability and water repellency of the structured surfaces. An increase in the nanostructure surface roughness facilitated a transition in the dynamic water droplet behavior from anisotropic/pinned to anisotropic/rollable, and to isotropic/rollable states. These transitions resulted from an increase in the degree of discontinuities in the three-phase contact line due to trapped air beneath the liquid. Our findings provide an understanding on the anisotropic water droplet rolling properties of rice leaves and will be valuable for the design of other functional surfaces for applications in microfluidics, self-cleaning coatings, and drag-reducing coatings.

4. Experimental Section

Plant Materials and Growth Conditions: Rice (*Oryza sativa* cv. Japonica) plants were grown in the greenhouse (32 °C/25 °C day/night, RH 75%) for 60 days after transplanting. Leaf blades were sampled from the youngest fully developed leaves of each plant.

Fabrication of Anisotropic Wavy PDMS Substrates: PDMS substrates, 1 mm thick, were prepared by pouring Sylgard 184 (Dow Corning) in a 10:1 ratio (by weight) of elastomer base to curing agent into a Petri dish, followed by curing at 60 °C for 4 h. The fully cured PDMS films with rectangular dimensions (40 mm × 10 mm) were clamped onto a custom-made stage and uniaxially stretched prior to placement in a UVO chamber (Jelight 42-220, 28 mW/cm^2) for 1 h. After UVO treatment, the strain was released from the PDMS substrate.

Preparation of the Water-Repellent Nanostructured Films: Nanostructured organic/inorganic films were easily prepared using the electrostatic self-assembly of SiO_2 nanoparticles (SN, 11 nm diameter, Sigma-Aldrich) and poly(allylamine hydrochloride) (PAH, $\overline{M}_w$ = 70 000 g/mol, Sigma-Aldrich) at room temperature. Prior to the first deposition of SN, polyelectrolyte prelayers were deposited onto the UVO-treated PDMS surface to facilitate the preparation of a dense SN layer. The PDMS substrate was immersed in a 40 mM PAH solution (pH 7.0) for 5 min and rinsed with DI water in three separate bottles. The substrate was then softly dried using a nitrogen stream. The PAH-modified PDMS was alternately dipped in a 40 mM poly(sodium 4-styrenesulfonate) (PSS, $\overline{M}_w$ = 70 000 g/mol, Sigma-Aldrich) solution and a PAH solution for 5 min, and then rinsed with DI water in three separate bottles, each for 1 min. The PDMS substrate was then dried under a nitrogen gas stream, and these procedures were repeated 5 times. The $(PAH/PSS)_5$-coated PDMS substrate was alternately immersed in PAH solution and 0.05 wt% SN solution (pH 4.5) for 5 min, then rinsed with DI water in three separate bottles, each for 1 min. Each substrate was then softly dried using a nitrogen stream. The substrates were allowed to dry in a vacuum oven at 60 °C overnight, then positioned in a vacuum desiccator with (tridecafluoro-1,1,2,2-tetrahydrooctyl)dimethylchlorosilane (500 μL, Gelest) for 12 h. The substrates were removed from the desiccators then rinsed with ethanol and blown dry under a stream of nitrogen.

Surface Characterization: The morphologies of the samples were examined by FESEM (Hitachi S-4200) at 4 kV. Three-dimensional images and the RMS roughness values of the prepared surfaces were

© 2013 WILEY-VCH Verlag GmbH & Co. KGaA, Weinheim

obtained by CLSM (LEXT OLS3100, Olympus). The water contact angles and roll-off angles were measured to characterize the wettability of the prepared substrates using a contact angle meter (SEO 300A, SEO Co.) under saturated humidity conditions (see the Supporting Information, Figure S1a). In situ images of the interface between the fabricated surfaces and the water droplets were collected by optical microscopy (Axioplan, Zeiss).

Supporting Information

Supporting Information is available from the Wiley Online Library or from the author.

Acknowledgements

This work was supported by a grant (Code No. 2011K000176) from the Center for Nanostructured Materials Technology under the 21st Century Frontier R&D Programs and a grant (Code No. 2011-0031628) from the Center for Advanced Soft Electronics under the Global Frontier Research Program of the Ministry of Education, Science and Technology, Korea.

Received: June 8, 2012
Revised: August 23, 2012
Published online: September 7, 2012

[1] H. Gau, S. Herminghaus, P. Lenz, R. Lipowsky, *Science* **1999**, *283*, 46.
[2] B. Zhao, J. S. Moore, D. J. Beebe, *Science* **2001**, *291*, 1023.
[3] M. Morita, T. Koga, H. Otsuka, A. Takahara, *Langmuir* **2005**, *21*, 911.
[4] A. M. Higgins, R. A. L. Jones, *Nature* **2000**, *404*, 476.
[5] M. Gleiche, L. F. Chi, H. Fuchs, *Nature* **2000**, *403*, 173.
[6] Z. Yoshimitsu, A. Nakajima, T. Watanabe, K. Hashimoto, *Langmuir* **2002**, *18*, 5818.
[7] J. Y. Chung, J. P. Youngblood, C. M. Stafford, *Soft Matter* **2007**, *3*, 1163.
[8] P. C. Lin, S. Yang, *Soft Matter* **2009**, *5*, 1011.
[9] N. A. Malvadkar, M. J. Hancock, K. Sekeroglu, W. J. Dressick, M. C. Demirel, *Nat. Mater.* **2010**, *9*, 1023.
[10] M. J. Hancock, K. Sekeroglu, M. C. Demirel, *Adv. Funct. Mater.* **2012**, *22*, 2223.
[11] L. Ionov, N. Houbenov, A. Sidorenko, M. Stamm, S. Minko, *Adv. Funct. Mater.* **2006**, *16*, 1153.
[12] D. Y. Xia, L. M. Johnson, G. P. Lopez, *Adv. Mater.* **2012**, *24*, 1287.
[13] W. Barthlott, C. Neinhuis, *Planta* **1997**, *202*, 1.
[14] Q. Cong, G.-H. Chen, Y. Fang, L.-Q. Ren, *J. Bionic Eng.* **2004**, *1*, 249.
[15] G. S. Watson, B. W. Cribb, J. A. Watson, *ACS Nano* **2010**, *4*, 129.
[16] L. Feng, S. H. Li, Y. S. Li, H. J. Li, L. J. Zhang, J. Zhai, Y. L. Song, B. Q. Liu, L. Jiang, D. B. Zhu, *Adv. Mater.* **2002**, *14*, 1857.
[17] J. Gao, Y. L. Liu, H. P. Xu, Z. Q. Wang, X. Zhang, *Langmuir* **2009**, *25*, 4365.
[18] F. X. Zhang, H. Y. Low, *Langmuir* **2007**, *23*, 7793.
[19] D. F. Zhu, X. A. Li, G. Zhang, X. Zhang, X. M. Zhang, T. Q. Wang, B. Yang, *Langmuir* **2010**, *26*, 14276.
[20] D. Wu, J. N. Wang, S. Z. Wu, Q. D. Chen, S. A. Zhao, H. Zhang, H. B. Sun, L. Jiang, *Adv. Funct. Mater.* **2011**, *21*, 2927.
[21] N. Bowden, S. Brittain, A. G. Evans, J. W. Hutchinson, G. M. Whitesides, *Nature* **1998**, *393*, 146.
[22] K. Efimenko, M. Rackaitis, E. Manias, A. Vaziri, L. Mahadevan, J. Genzer, *Nat. Mater.* **2005**, *4*, 293.
[23] E. P. Chan, E. J. Smith, R. C. Hayward, A. J. Crosby, *Adv. Mater.* **2008**, *20*, 711.
[24] S. Yang, K. Khare, P. C. Lin, *Adv. Funct. Mater.* **2010**, *20*, 2550.
[25] G. Decher, *Science* **1997**, *277*, 1232.
[26] L. Zhai, F. C. Cebeci, R. E. Cohen, M. F. Rubner, *Nano Lett.* **2004**, *4*, 1349.
[27] J. Park, L. D. Fouche, P. T. Hammond, *Adv. Mater.* **2005**, *17*, 2575.
[28] J. T. Han, Y. Zheng, J. H. Cho, X. Xu, K. Cho, *J. Phys. Chem. B* **2005**, *109*, 20773.
[29] H. S. Lim, J. T. Han, D. Kwak, M. H. Jin, K. Cho, *J. Am. Chem. Soc.* **2006**, *128*, 14458.
[30] D. Kwak, J. T. Han, J. H. Lee, H. S. Lim, D. H. Lee, K. Cho, *Surf. Sci.* **2008**, *602*, 3100.
[31] C. G. L. Furmidge, *J. Colloid Sci.* **1962**, *17*, 309.
[32] R. N. Wenzel, *Ind. Eng. Chem.* **1936**, *28*, 998.
[33] A. B. D. Cassie, S. Baxter, *Trans. Faraday Soc.* **1944**, *40*, 546.
[34] A. Lafuma, D. Quere, *Nat. Mater.* **2003**, *2*, 457.
[35] W. Chen, A. Y. Fadeev, M. C. Hsieh, D. Oner, J. Youngblood, T. J. McCarthy, *Langmuir* **1999**, *15*, 3395.
[36] C. W. Extrand, *Langmuir* **2003**, *19*, 3793.
[37] F. Shi, Z. Q. Wang, X. Zhang, *Adv. Mater.* **2005**, *17*, 1005.
[38] J. T. Han, X. Xu, K. Cho, *Langmuir* **2005**, *21*, 6662.
[39] H. S. Lim, S. G. Lee, D. H. Lee, D. Y. Lee, S. Lee, K. Cho, *Adv. Mater.* **2008**, *20*, 4438.
[40] S. G. Lee, D. Y. Lee, H. S. Lim, D. H. Lee, S. Lee, K. Cho, *Adv. Mater.* **2010**, *22*, 5013.
[41] S. Pechook, B. Pokroy, *Adv. Funct. Mater.* **2012**, *22*, 745.
[42] Y. Xiu, L. Zhu, D. W. Hess, C. P. Wong, *Nano Lett.* **2007**, *7*, 3388.
[43] X. F. Gao, X. Yao, L. Jiang, *Langmuir* **2007**, *23*, 4886.

© 2013 WILEY-VCH Verlag GmbH & Co. KGaA, Weinheim